Atmospheric Research 167 (2016) 77–88

Contents lists available at ScienceDirect

Atmospheric Research

journal homepage: www.elsevier.com/locate/atmos

Modeling study of surface ozone source-receptor relationships in East Asia

Jie Li [a,*], Wenyi Yang [a,b], Zifa Wang [a], Huansheng Chen [a], Bo Hu [a], Jianjun. Li [c], Yele. Sun [a], Pingqing Fu [a], Yuqia Zhang [a,d]

[a] LAPC, Institute of Atmospheric Physics, Chinese Academy of Sciences, Beijing 100029, People's Republic of China
[b] University of Chinese Academy of Sciences, Beijing 100049, People's Republic of China
[c] China National Environmental Monitoring Centre, Beijing 100012, People's Republic of China
[d] Chengdu University of Information Technology, Sichuan 610225, People's Republic of China

ARTICLE INFO

Article history:
Received 23 February 2015
Received in revised form 23 June 2015
Accepted 17 July 2015
Available online 26 July 2015

Keywords:
Source–receptor relationships
Surface ozone
East Asia
Chemical transport model
Long-range transport

ABSTRACT

Ozone source–receptor relationships over East Asia have been quantitatively investigated using a chemical transport model including an on-line tracer-tagged procedure, with a particular focus on the source regions of different daily ozone mixing ratios. Comparison with observations showed that the model reproduced surface ozone and tropospheric nitrogen dioxide column densities. Long-range transport from outside East Asia contributed the greatest fraction to annual surface ozone over remote regions, the Korean peninsula, and Japan, reaching 50%–80% of total ozone. Self-contributions accounted for 5%–20% ozone in the Korean peninsula and Japan, whereas the contribution of trans-boundary transport from photochemical production in China was less than 5%–10%. At extra-high ozone levels, self-contributions reached 50%–60% in the Korean peninsula. Ozone source–receptor relationships showed high seasonal variability over East Asia. Significant transport was also found between sub-regions in China, which presents a great challenge to policy-makers because most current control strategies are confined to specific regions.

1. Introduction

Tropospheric ozone (O_3) is a secondary air pollutant produced through thousands of photochemical reactions and has significant impacts on human health, ecosystems, and climate change (Ahamad, et al., 2014; Zhang, R. et al., 2013). Recently, tropospheric ozone in East Asia has attracted increasing worldwide attention due to the dramatic growth in its precursor emissions, in contrast to their significant decrease in Europe and lack of change in North America (Naja and Akimoto, 2004). This increase in ozone could affect hemispheric-scale atmospheric oxidizing capacity and formation of other pollutants (e.g., sulfates, nitrates, and other secondary aerosols) through reported long-range transport (Wild and Akimoto, et al., 2001). Therefore, quantitative estimation of ozone sources in East Asia has been an essential issue in understanding global-scale atmospheric environment and climate change. However, the high complexity of ozone formation in East Asia seems to be an impediment to understanding ozone source–receptor relationships (S–R relationships). For example, ozone showed a 2.6 ± 2.0%/y trend in the northwestern Pacific (Lee et al., 1998), but did not show the expected high and increasing rates at rural sites in source regions (e.g., China), where a decreasing trend of averaged concentration with enhanced variability was reported. Observations at Lin'an showed that averaged and median concentrations of surface ozone decreased by 0.37 ppbv/y and 0.56 ppbv/y since 1991, although monthly highest 5% increased at a rate of 0.68 ppb/y due to increasing nitrogen oxides (Xu et al., 2008). Furthermore, simulated summer mean ozone in the northeastern Pacific showed a marked overprediction by 30 ppbv (Itahashi et al., 2013). This inconsistency between long-term background ozone trends in industrialized regions and in the western Pacific has been reported by Naja and Akimoto (2004), who found that regional ozone pollution from China did not increase during the 1990s despite the very rapid increase in NO_x emissions over China [Naja and Akimoto, 2004].

Compared with primary pollutants like CO, one difficulty in estimating ozone source–receptor relationships is how to consider the impact of the strong nonlinearity of O_3–VOC–NO_x chemistry. Yamaji et al. (2006), using the widely used brute-force method, estimated that Asian anthropogenic emissions contributed 40%–70% of surface ozone in East Asia. However, this conclusion was greatly influenced by nonlinear O_3 response to the magnitude of the perturbation range. Recently, a so-called decoupled direct method (DDM) and higher-order DDM (HDDM) were used to assess source–receptor relationships in East Asia, which was expected to reduce the impact of nonlinear O_3 response to emission perturbations in the simulation by calculating the higher-order sensitivity coefficients (Itahashi et al., 2013). However, their

* Corresponding author.
E-mail address: lijie8074@mail.iap.ac.cn (J. Li).

http://dx.doi.org/10.1016/j.atmosres.2015.07.010

simulation greatly overestimated summer surface ozone in mid-latitude rural sites over East Asia by 30 ppbv (50%–80%), which may cause errors in source–receptor relationships.

Another approach, called the "on-line tracer-tagged" method, calculated the contribution of chemically created ozone inside specified regions to the modeling domain. This approach facilitated assessment of contributions from different regions to ozone in East Asia by avoiding uncertainties from the nonlinearity of O_3–VOC–NO_x chemistry (Grewe et al., 2004). Using this approach, Li et al. (2008) quantitatively analyzed ozone source–receptor relationships over central and eastern China in June. Furthermore, Nagashima et al. (2010) extended this study from one month to six full years (2000–2005) using a global chemical transport model (CHASER) with 2.8° × 2.8° horizontal resolution and found that long-range transport brought 20% of observed ozone to Japan. However, coarse resolution affected the accuracy of their estimates of S–R relationships. Wild and Prather (2006) found that coarse resolution resulted in overestimation of O_3 production in polluted regions and had significant implications for source-attribution studies of tropospheric O_3. Therefore, studies of long-term quantitative estimation of ozone S–R relationships at fine resolution over East Asia are necessary. Unfortunately, current regional simulations have been mainly restricted to several-day episodes (Itahashi et al., 2013).

In this study, a regional chemical transport model with an on-line tracer-tagged module was used to estimate one-year ozone S–R relationships in East Asia in 2010. Importantly, S–R relationships for different surface O_3 concentrations classified into 2-ppbv increments, which have rarely been presented in previous simulations using regional models, were also discussed. These estimates also provided a base for assessing the effectiveness of the unprecedented "Atmospheric Pollution Prevention Action Plan", which was recently officially announced and which serves as a guide for national efforts to prevent and control air pollution in 2013–2017. In this Plan, unprecedented control measures will be implemented, and the Government's mandatory air quality objectives for 2017 were explicitly revealed to the public.

2. Model description and setup

2.1. Model description

In this study, a so-called Nested Air Quality Prediction Modeling System (NAQPMS) was used, which was developed by the Institute of Atmospheric Physics, Chinese Academy of Sciences (Wang et al., 2001). NAQPMS is a fully modularized 3-D chemical transport model derived from the Weather Research and Forecasting model (WRF, version 3.5, Skamarock and Klemp, 2008). The physical and chemical evolution of reactive pollutants in the atmosphere is reproduced by solving the mass balance equation in terrain-following coordinates. The carbon-bond mechanism Z (CBM-Z), which is composed of 71 species and 134 chemical reactions, is implemented in NAQPMS to simulate gaseous chemistry (Zaveri and Peters, 1999). The RADM mechanism for aqueous chemistry and wet deposition involves 22 species. The ISSOROPIA1.7 model is embedded into NAQPMS to calculate the composition and phase of an ammonia–sulfate–nitrate–chloride–sodium–water inorganic aerosol (Nenes et al., 1998). Secondary organic aerosols (SOA) are currently treated by a bulk two-product yield parameterization (Odum et al., 1997). Aerosol optical depths at 550 nm are converted from mass concentrations using a so-called external mixture-based "reconstructed extinction coefficient method" proposed by James and Malm (2000). An accurate radiative-transfer model (TUV version 4.5) with an eight-stream discrete ordinate solver was online-coupled with NAQPMS to evaluate the effects of aerosols on photolysis frequencies and tropospheric oxidants (TUV, Madronich, 1989; Li et al., 2011). As for simulation of heterogeneous chemical processes, 12 species and 28 reactions involving dust, sea salt, sulfate, and black carbon were included. This model has been successfully used to simulate mixing between dust and anthropogenic gaseous pollutants in East Asia (Li et al., 2012). The advection scheme used an accurate mass-conservative, peak-preserving algorithm (Waleck and Aleksic, 1998). The dry deposition velocity was parameterized using a scheme proposed by Wesely (1989).

Traditionally, the brute-force method, in which the contributions of certain specified regions are obtained by comparing the differences between two model simulations with different emissions, has been used to evaluate source–receptor relationships in modeling studies. However, recent studies have shown that this method underestimates total ozone by 40% at a global scale and 10%–20% over East China (Grewe, 2004). To avoid this problem, an on-line tagged tracer module is used in NAQPMS to identify the proportion of O_3 moving from a pollutant-producing region to a receptor area. In this module, O_3 is tagged by the geographical location where it was produced. The contributions from top and lateral boundaries and from initial conditions are also evaluated. Compared with the classical sensitivity approach, the tagged tracer method is more efficient in that it requires only one run and the contribution of each source region is strictly positive. A detailed description can be found in previous work (Li et al., 2008). Noted that we mainly addresses ozone itself in this study (direct transport), and photochemical production of precursors from source regions in the transport (indirect transport) was included the contribution of ozone production region. NAQPMS has been widely used to assess the impact of regional transport of ozone and aerosols on high-pollution episodes and on long-term air quality in East Asia (Li et al., 2009, 2012, 2013; Ge et al., 2014).

2.2. Modeling setup

The horizontal model domain, which is 8000 × 5800 km^2 on a Lambert conformal map projection with 81-km horizontal resolution, is shown in Fig. 1. Vertically, the grid structure consists of 20 layers from the surface to the model top (20 km a.s.l.), with the lowest six layers below 1 km. The initial and boundary conditions for this simulation were taken from monthly averaged 2.8° × 2.8° output from a global chemistry and transport model (MOZART-2) (Horowitz et al., 2003).

The anthropogenic emission inventory for China used in this study was obtained from Zhao et al. (2013) with 0.25° × 0.25° resolution in 2009 and was based on Chinese energy statistics, emission factors, and other economic information. Anthropogenic emissions in other countries were taken from the bottom-up Regional Emission inventory in ASia (REAS2.1) (Kurokawa et al., 2013). Biomass-burning emissions in China and Southeast Asia were obtained from Cao et al. (2005) and GFEDV3 respectively. Both of these are constrained by MODIS satellite data. Natural hydrocarbon emissions were derived from the Global Emissions Initiative (GEIA) (Guenther et al., 1995).

Eleven ozone production regions in East Asia were tagged, as were initial conditions, lateral boundaries, and stratospheric ozone. The ozone production regions included seven sub-regions in China, Korea, Japan, the western Pacific, and parts of Southeast Asia, India, and eastern Siberia. Their geographical locations are shown in Fig. 1. Table 1 gives a detailed description of area, population, and emissions in the study area. North China (NCHN), East China (ECHN), and Central China (CCHN) are rapidly developing regions in China, which accounted for 62% of NO_x and 42% of VOC emissions in China from only 16% of its area. In particular, ECHN is located along the coastline of the Asian continent, which favors trans-boundary transport from China to the western Pacific. The simulation period was December 2009 to December 2010, with a one-month spin-up time. The basic integration time step for NAQPMS was 5 min. In the next section, the model's ability to simulate ozone is evaluated by comparing model results with observations (including ground and satellite data).

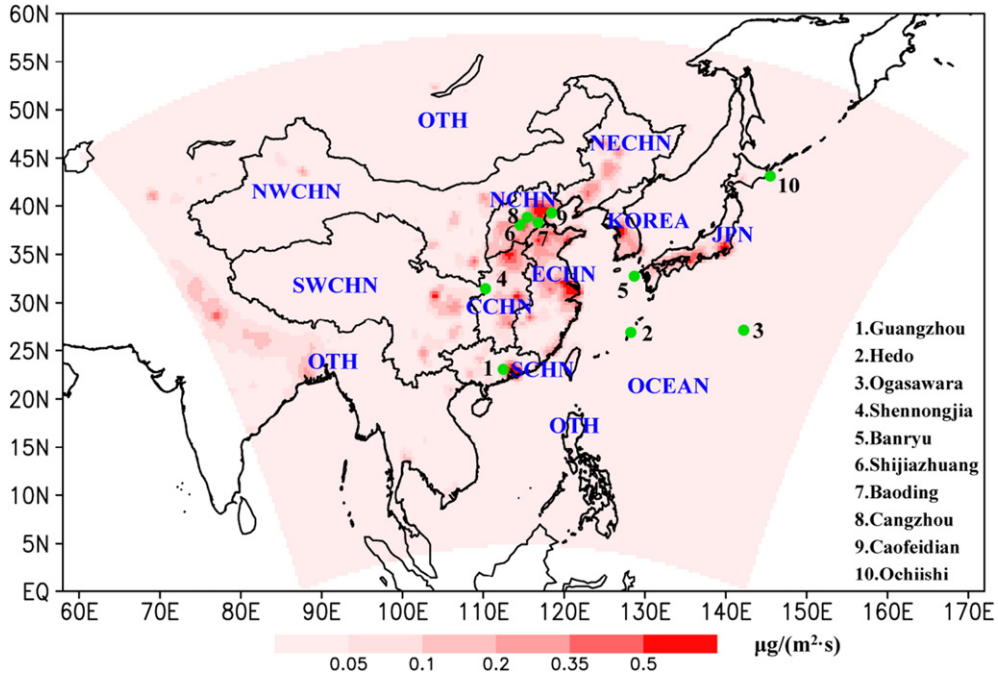

Fig. 1. Model domain for NAQPMS with NO_x emission rates (shaded). Also shown are tagged O_3 production regions (blue capital letters). The solid green circles represent the locations of the observation sites.

3. Results and discussion

3.1. Regional model versus observations

3.1.1. Surface ozone

Fig. 2 presents simulated and observed monthly average surface ozone at various sites over East Asia from the Beijing–Tianjing–Hebei Atmospheric Environment Monitoring Network (BTHAEMN) (Xin et al., 2010) (Shijiazhuang, Baoding, Cangzhou, and Caofeidian), the Acid Deposition Monitoring Network in East Asia (EANET) (Hedo, Ogasawara, Banryu, and Ochiishi) (http://www.wanet.cc/product.html), the China National Environment Monitoring Centre (CNEMC) (Shennongjia), and the Pearl River Delta regional air quality monitoring network (Guangzhou). The observations were made in 2010, except for the CNEMC data which were available only in 2011. These stations were chosen for their geographical coverage of both the major industrialized (China and Japan) and downwind (western Pacific) regions, as well as their representativeness of a range of latitudes (20°–45°N). In general, the model simulated magnitudes and seasonal variations reasonably well. The normalized mean biases (NMB) between the daily mean observations and the model calculated values ranged from −5% to 23%, and the root mean square error (RMSE) was approximately 10 ppbv. At most mid-latitude stations from central China (site name: Shennongjia) to the northwestern Pacific, NAQPMS reproduced the observed bimodal behavior in spring and fall reasonably well. In the North China Plain (Shijiazhuang, Baoding, Cangzhou, and Caofeidian), both the simulation and the observations showed the June maximum of ozone mixing ratios, which is due to enhanced chemical production in summertime.

Fig. 3 shows the observed and simulated probability distributions (2 ppbv per bin) of daily surface ozone at the various stations in 2010. Interestingly, although some sites showed similar seasonal variation (bimodal behavior in spring and fall), their probability distributions were completely different. On the Asian continent (Shennongjia) and in Japan (Ochiishi and Banyu), ozone probability showed a single-peak (30–50 ppbv) distribution. In contrast, a bimodal distribution with peaks at 10–20 ppbv and 40–50 ppbv dominated at low-latitude sites far away from continents (Hedo and Ogasawara). This bimodal distribution reflected the impact of continental and oceanic air masses on these sites in different seasons. NAQPMS reproduced these ozone probability distribution patterns well (Fig. 2). At industrialized sites (Shijiazhuang, Baoding, Changzhou, Caofeidian, and Guangzhou), probabilities were highest on days with low ozone (below 20 ppbv) and gently decreased as ozone mixing ratios increased. This phenomenon was caused by titration of saturated nitrogen oxides (NO_x) in these regions.

Table 1
Tagged ozone production regions in the model domain and their anthropogenic emissions in this study.

Regions	Area (10^3 km^2)	NO_x emissions[a] (Tg/year)	NMVOC emissions (Tg/year)
East China (ECHN)	794.6	8.5	12.5
South China (SCHN)	491.5	2.2	6.7
Central China (CCHN)	566.2	3.8	7.0
North China (NCHN)	156.2	4.2	3.7
Northeast China (NECHN)	788.1	2.5	5.0
Northwest China (NWCHN)	4300.0	3.2	7.7
Southwest China(SWCHN)	2342.3	2.6	8.3
Korea	219.7	1.3	0.8
Japan	377.7	2.2	1.5
Ocean		0.0	0.0

[a] Emissions in China and other countries are based on the year 2009 and 2007, and taken from Zhao et al. (2013) and Kurokawa et al. (2013), respectively.

3.1.2. Satellite tropospheric column nitrogen dioxide (NO_2)

To obtain a more comprehensive assessment of ozone precursors (NO_x), the tropospheric column NO_2 from the SCIMACHY satellite was compared with the model results. The SCIMACHY remote-sensing measurements provided column densities over the troposphere after correction for vertical sensitivity from slant column densities to vertical column densities (VCD) (Stammes, 2001). To maintain consistency in this comparison, the same definition of the tropopause (2 K/km) was

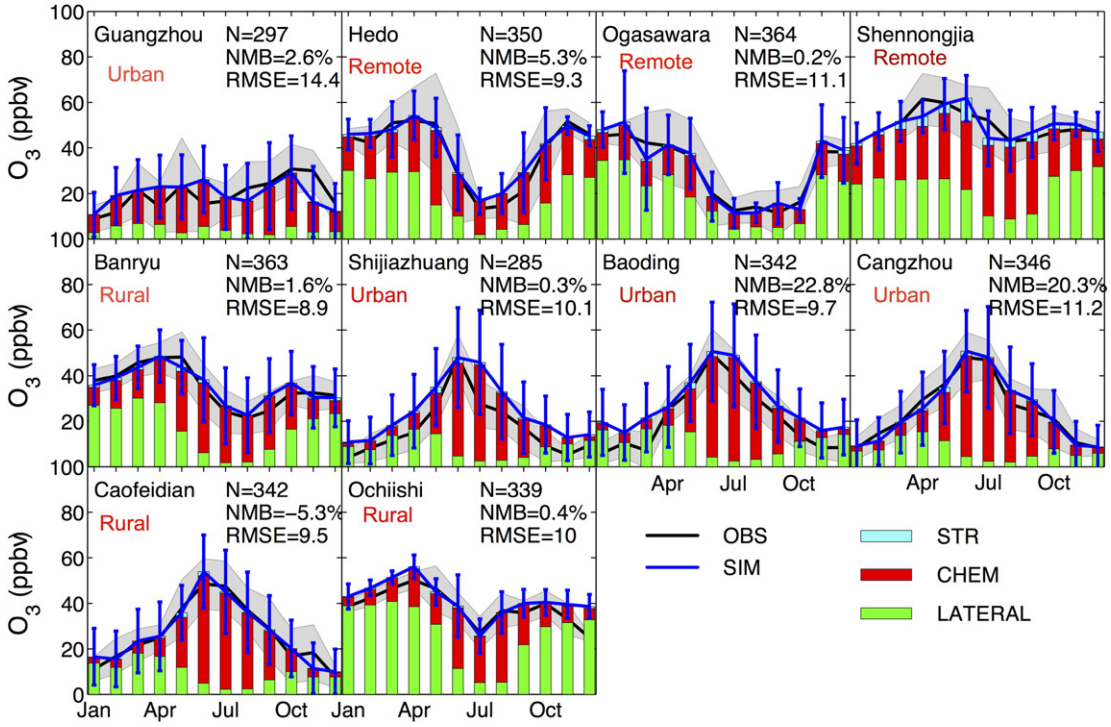

Fig. 2. Observed (black line) and simulated (blue line) monthly mean surface O_3 with standard deviation in 2010. Also shown are contributions from the stratosphere (sky-blue column) and from chemical production (red column) in East Asia, as well as lateral boundary conditions (green column). The red characters represent the type of sites (Urban, Rural and Remote).

used. The simulated tropospheric NO_2 column densities (VCD_{NO2}) in molecule cm^{-2} were calculated according to the following formula:

$$VCD_{NO2} = \sum_{i=1}^{20} \frac{P_i \times D_i \times A \times C_{i(NO2)}}{R \times T_i \times 10^9 \times 10^4}$$

where P_i, D_i, T_i and $C_{i(NO2)}$ are the simulated pressure (Pa), layer depth (m), temperature (K), and NO_2 concentration (ppbv) respectively of layer i at UTC 3:00 for consistency with the overpass time of the ENVISAT satellite in China (Boersma et al., 2011), and R and A are the gas constant (8.34 J $mole^{-1}$ K^{-1}) and Avogadro's number (6.02×10^{23}).

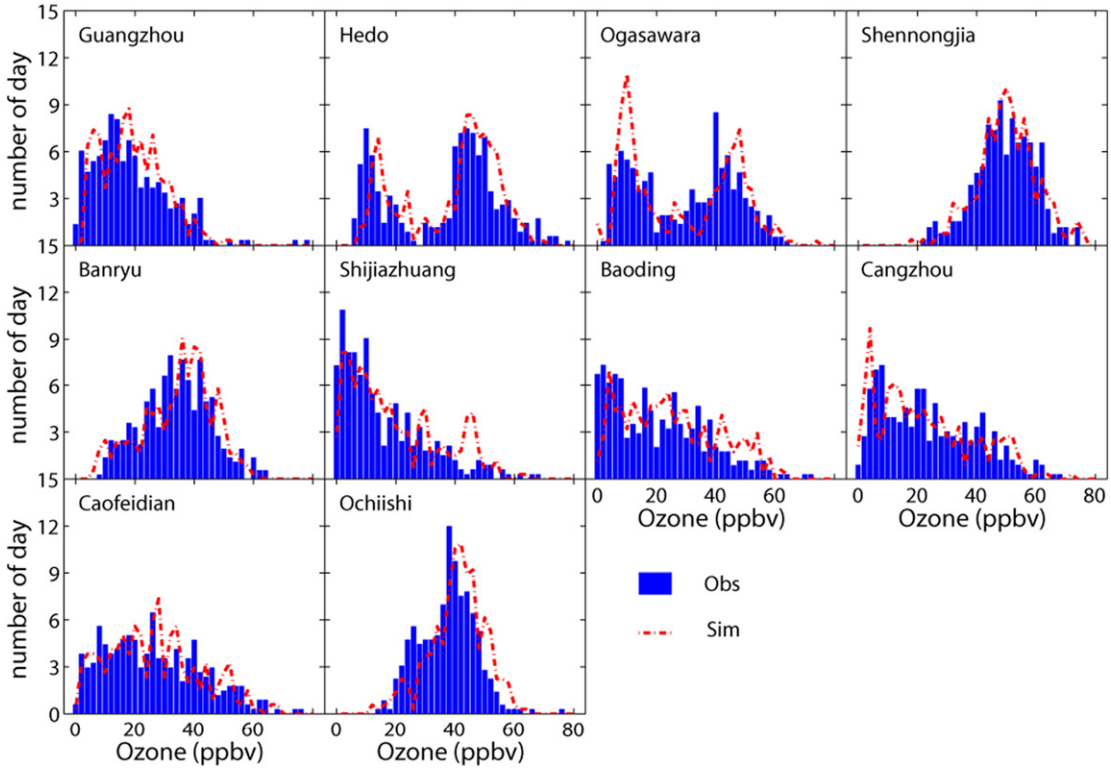

Fig. 3. Observed (blue column bars) and simulated (red dashed lines) probability distribution (2 ppbv per bin) of daily surface ozone at various stations in 2010.

Fig. 4 shows the observed and modeled seasonal tropospheric column densities of NO_2 in moles/cm^2 over East Asia in 2010. Both NAQPMS and SCIMACHY showed high VCD over the North China Plain, the Yangtze River Delta, and the Pearl River Delta regions in China. VCD in the regions near Seoul and Tokyo also exceeded 1.5×10^{16} moles/cm^2 in all four seasons. In winter and spring, the North China Plain and the Yangtze River Delta were merged into one high-VCD plume with more than 2.5×10^{16} moles/cm^2. In summer, this plume broke up, and high VCD was scattered over several megacity clusters. These features were all successfully reproduced by NAQPMS.

Overall, this model evaluation using observed surface ozone and satellite NO_2 data shows that NAQPMS captured the temporal and spatial ozone variations over East Asia. This reasonable performance gives some confidence in the assessment of model-derived contributions from various source regions.

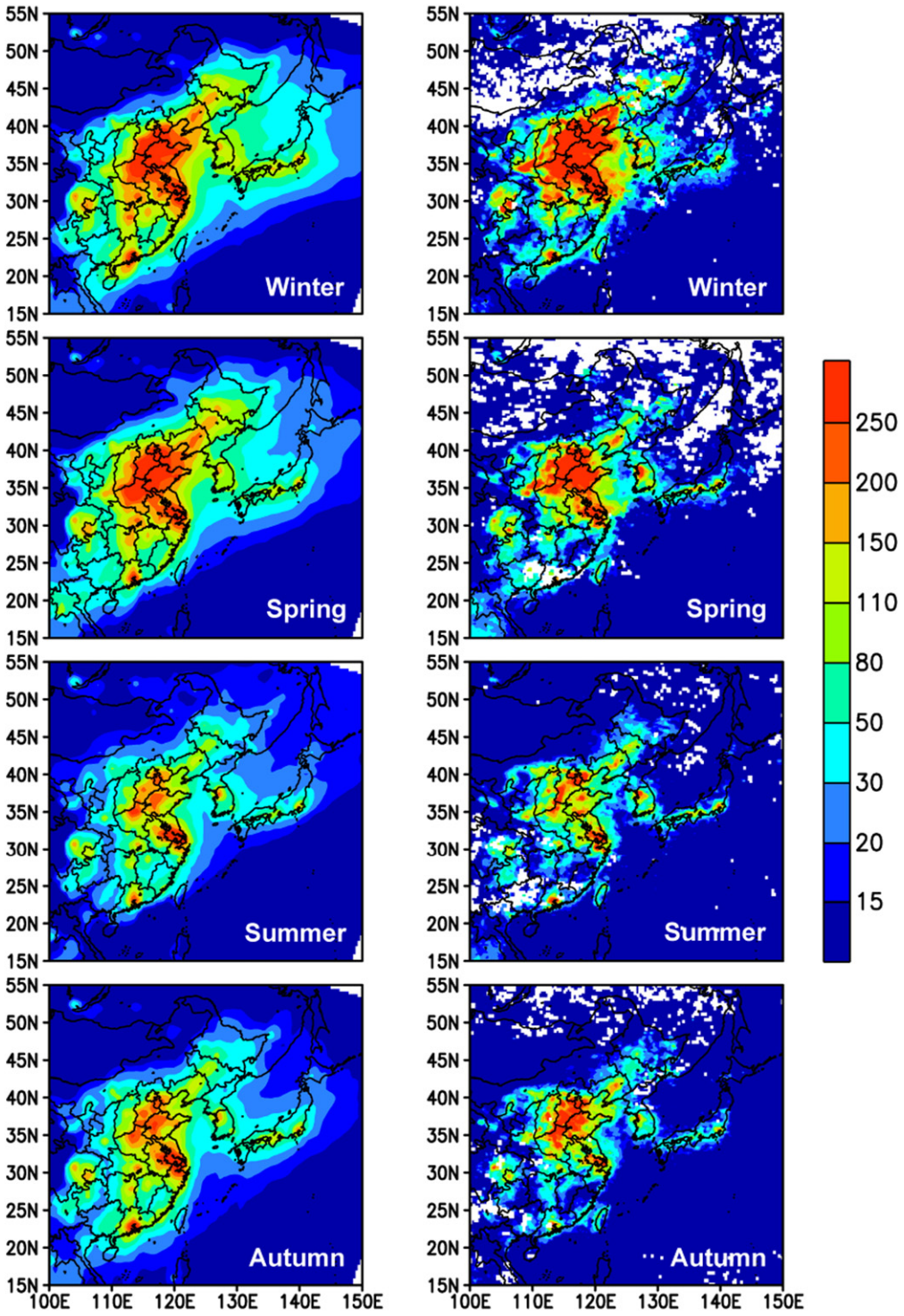

Fig. 4. Comparison between seasonal mean calculated tropospheric NO_2 columns (1×10^{14} moles/cm^2) from NAQPMS (left panels) and satellite measurements from SCIMACHY (right panels) in 2010.

3.2. Annual surface ozone and its source–receptor relationships over East Asia

Fig. 5 shows the spatial distributions of simulated annual mean surface O_3 and contributions from tagged source regions (China, the Korean peninsula, Japan, the western Pacific Ocean, and top and lateral boundary conditions) in 2010. It was found that surface ozone in industrialized regions (NCHN, ECHN, and megacities in Korea and Japan) exhibited lower mixing ratios (15–25 ppbv) than the northwestern Pacific and other remote regions (e.g., western China and Mongolia) (35–45 ppbv). This spatial distribution pattern was consistent with ground-level observations, but in contrast with simulated surface O_3 predictions in 2000–2005 using a global model (Nagashima et al., 2010), in which surface ozone in East China was the highest (40–80 ppbv) and was much higher than in remote regions. This effect was likely caused by the coarse resolution in the global model, leading to overestimation of O_3 production in polluted regions (Wild and Prather, 2006). In addition, the different treatment of the impact of aerosols by photolysis effects and heterogeneous chemistry in different models is likely another cause, as reported by Wild and Prather (2006).

Long-range transport from outside East Asia (lateral conditions and stratospheric ozone over East Asia) contributed the most to surface ozone over most regions in East Asia (Fig. 5e). In the western Pacific, Mongolia, eastern Siberia, and northeastern China (NECHN), its contribution reached 60%–80% (25–45 ppbv). It also contributed 50%–70% of surface ozone, with an increasing trend from west to east, in the Korean peninsula and Japan. Over industrialized regions in China (CCHN, ECHN, and SCHN), this long-range transport from outside East Asia contributed only 5–10 ppbv (20%–30%). This phenomenon was likely caused by high NO_x emissions in China. On the one hand, saturated NO_x in winter titrated long-range transported ozone. On the other hand, intensive photochemical reactions in summer produced more O_3 in this region. O_3 produced in eastern China (NCHN, ECHN, and SCHN) was mostly confined to that region, with a contribution of 10–25 ppbv (30%–70%) (Fig. 5a). Over the Korean peninsula and Japan, O_3 produced in China contributed 2–5 ppbv (less than 5%–10%), and their self-contributions reached 5–8 ppbv (5%–20%) (Fig. 5b and c). O_3 produced in the Pacific Ocean significantly contributed to concentrations in the western Pacific, the Korean peninsula, and Japan, with a range of 5–15 ppbv (10%–40%) (Fig. 5d). Note that O_3 precursors in the Pacific Ocean came from China, the Korean peninsula, Japan, and Southeast Asia (Tang et al., 2003), and it is difficult to apportion these targeted O_3 precursors among these various source regions.

Fig. 6 shows the contributions of the targeted regions to various levels of surface daily ozone (0–100 ppbv, 2 ppbv per bin) in each grid cell within the Korean peninsula and western and eastern Japan. In the Korean peninsula, the contribution from long-range transport from outside East Asia was substantially restricted at ozone levels below 60 ppbv (with peaks at 35–40 ppbv), although it was the highest source on average (Fig. 6a). In contrast, the contribution from local photochemical production showed an increasing trend at greater ozone mixing ratios. At extra-high surface O_3 levels (exceeding 80 ppbv), it even reached 50%–60%, which was three or four times the value for low ozone (0–50 ppbv). The contribution of ozone produced in China and the Pacific Ocean remained stable, with magnitudes of 10% and 25% respectively. In western Japan (west of 138°E), extra-high surface O_3 (exceeding 80 ppbv) was caused by long-range transport from outside East Asia (70%) (Fig. 6b). This probably occurred because high ozone in the middle troposphere (300–500 hPa) at high latitudes was transported downward. Wu (2002) found that significant downward motion extended from western Japan eastward to the western North Pacific in some cases, whereas upward motion anomalies occurred over the Asian continent. Local photochemistry contributed 30% of the ozone in the 60–80 ppbv bins of total surface ozone, which was comparable with values from the Pacific Ocean. Cross-boundary contributions from China were only 5%. In eastern Japan, long-range transport from outside East Asia was the major source (60%–70%) when surface ozone was higher than 40 ppbv (Fig. 6c). This phenomenon was related

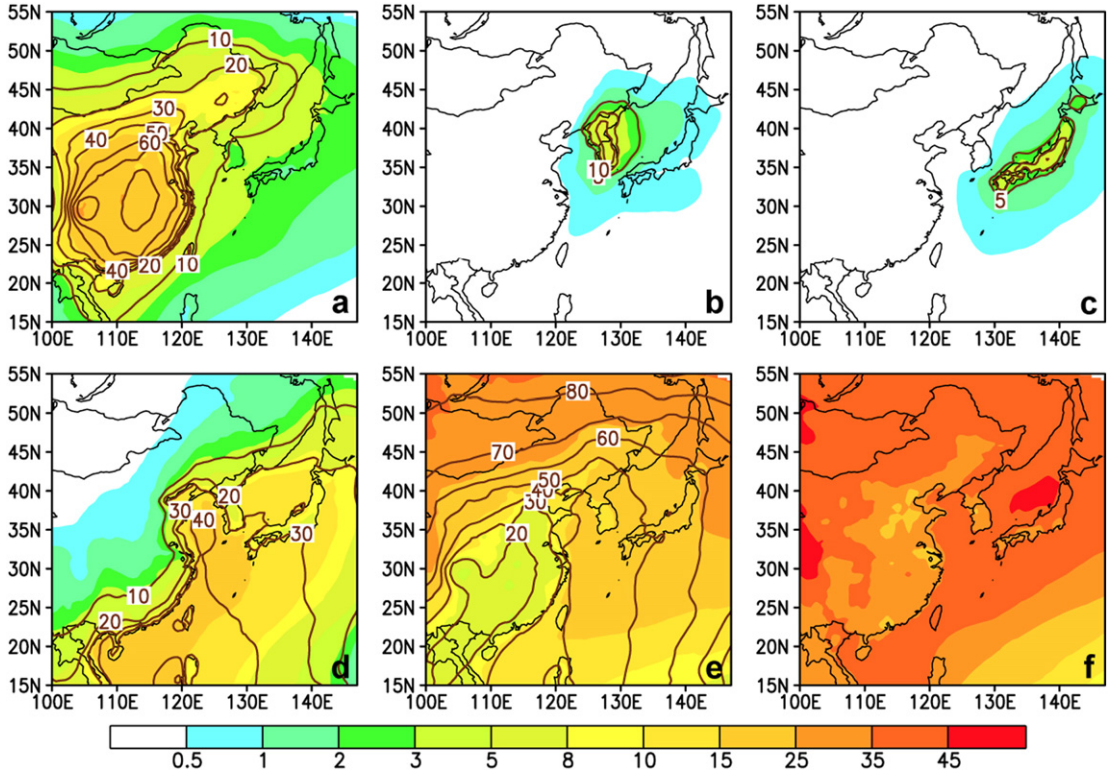

Fig. 5. Spatial distributions of simulated annual mean surface O_3 (f) and contributions from tagged source regions in 2010 (a: China, b: Korean peninsula, c: Japan, d: Ocean, e: top and lateral boundary conditions).

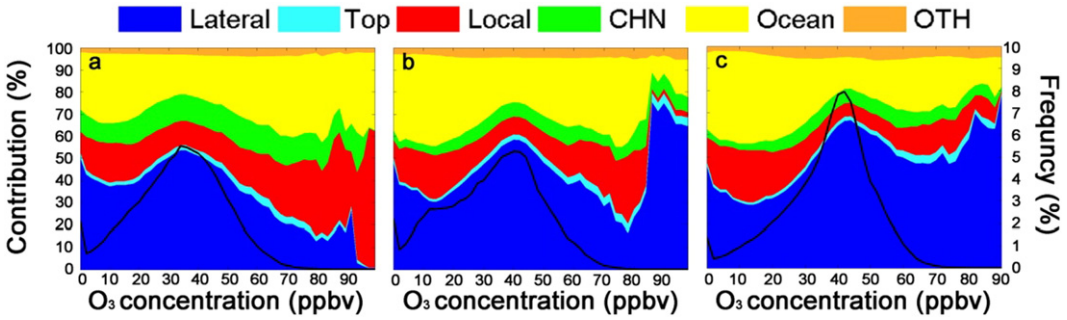

Fig. 6. Relative contributions of targeted regions to different levels of surface daily ozone (0–100 ppbv, 2 ppbv per bin) in each grid cell within the Korean peninsula (a), western Japan (b), and eastern Japan (c). Also shown is the probability distribution (2 ppbv per bin) of daily surface ozone.

to geographic location. Eastern Japan extends from 35°N to 45°N and is closer to the northern boundaries where ozone-mixing ratios were always greater than 40 ppbv (Horowitz et al., 2003).

3.3. Seasonal variation of surface ozone source–receptor relationships over East Asia

Fig. 7 illustrates simulated East Asian surface ozone mixing ratios in all seasons of 2010. In general, the mid-latitude parts of the northwestern Pacific (north of 25°N) exhibited a seasonal cycle with a spring maximum (~50 ppbv) and a summer minimum (~20–35 ppbv). In the North China Plain (NCHN and ECHN), the maximum of surface ozone appeared in summer, with 50–60 ppbv. As shown in Fig. 2, springtime ozone at sites in the northwestern Pacific (Hedo, Ogasawara, Banryu, and Ochiishi) came mostly from long-range transport across lateral boundaries (outside East Asia) (~30 ppbv); chemical production within the modeling domain contributed only 10–15 ppbv ozone. In contrast, the ozone summer maximum in NCHN and ECHN (Baoding, Shijiazhuang, Cangzhou, and Caofeidian) resulted mainly from chemical production in East Asia, which accounted for 90%. Compared with summer-maximum in NCHN, ozone in SCHN (Guangzhou site) in summer was much lower, which was caused by the dominated summer monsoon system in SCHN from the Indian Ocean and Pacific.

In detail, surface ozone in winter was present at 30–40 ppbv in East Asia except for industrialized regions in China, where ozone was only 10–20 ppbv due to titration of saturated NO_x. Because of the strong zonal pressure gradient between the Siberian High and the Aleutian Low, a strong O_3 outflow band from Siberia to the open Pacific was located between 25° and 45°N and passed through northern China (NCHN, ECHN, and NECHN), the Korean peninsula, and Japan. This indicated that these regions were largely influenced by their northern boundaries in winter. In spring, surface ozone increased in the whole domain due to the increase in solar radiation. Two high-ozone regions appeared in Siberia (Mongolia) and Japan. Due to the weakness of the

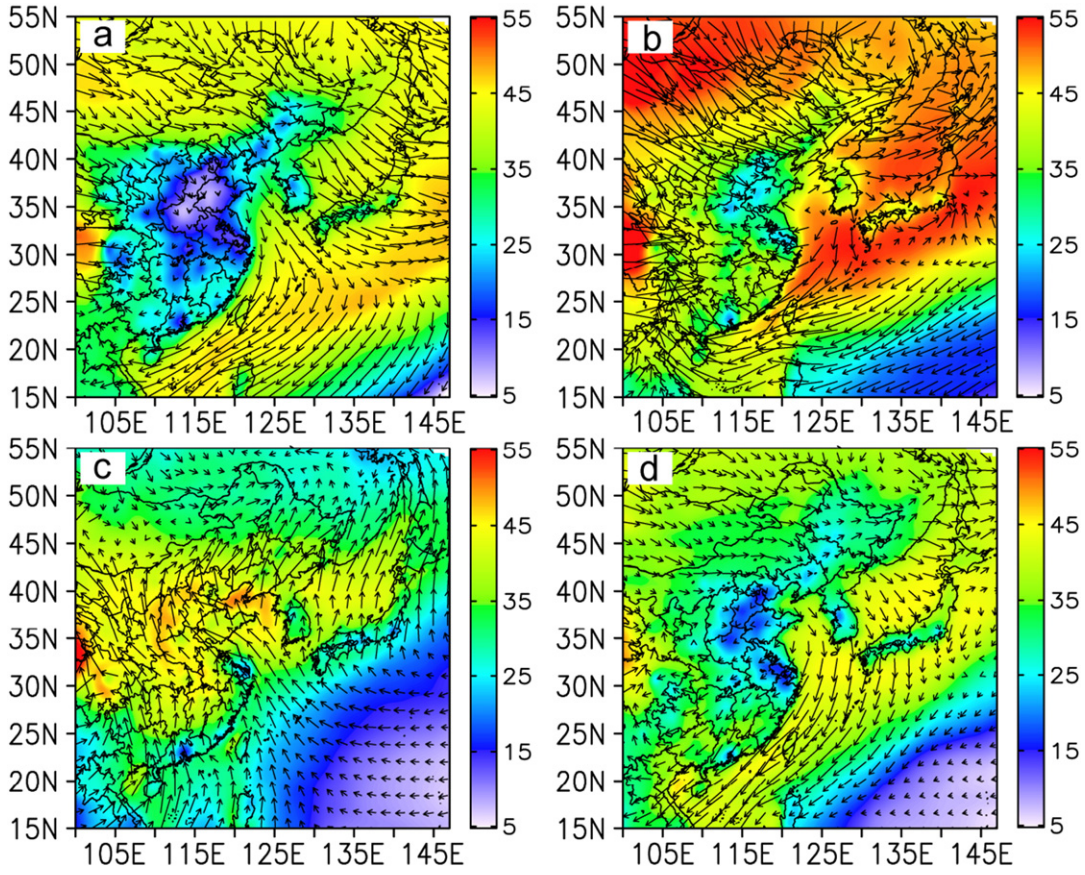

Fig. 7. Simulated East Asian surface ozone mixing ratios (ppbv) and transport flux (mol/(m^2 s)) in all seasons of 2010 (a: winter; b: spring; c: summer, d: fall).

Table 2
Surface ozone contributions (ppbv) and percentages (in brackets) from source regions to receptor regions over East Asia in spring 2010.

S/R	ECHN	SCHN	CCHN	NCHN	NECHN	NWCHN	SWCHN	CHN	Korea	Japan
Boundary	12.2(36.8)	8.9(25.5)	10.6(30.7)	20.6(64.1)	30.3(70.2)	36.5(78.7)	30.9(59.7)	28.9(64.7)	25.2(58.2)	29.3(62.4)
ECHN	10.9(33)	1.7(4.9)	3.8(11.1)	1.3(4.1)	0.7(1.6)	0.2(0.4)	0.2(0.4)	1.5(3.4)	1.2(2.8)	0.8(1.8)
SCHN	0.9(2.8)	8.4(24.1)	2.2(6.4)	0.2(0.6)	0.04(0.1)	0.1(0.2)	0.8(1.5)	0.9(2.1)	0.1(0.2)	0.05(0.1)
CCHN	1.4(4.1)	2.0(5.6)	12.4(36)	1.7(5.3)	0.2(0.4)	0.4(0.9)	0.9(1.7)	1.4(3.2)	0.3(0.6)	0.2(0.4)
NCHN	0.2(0.7)	0.1(0.2)	0.2(0.7)	3.7(11.5)	0.3(0.7)	0.2(0.4)	0.0(0.0)	0.3(0.6)	0.3(0.8)	0.2(0.5)
NECHN	0.2(0.7)	0.1(0.2)	0.05(0.1)	0.1(0.4)	4.0(9.2)	0.1(0.3)	0.0(0.0)	0.4(0.9)	1.9(4.4)	1.3(2.8)
NWCHN	0.4(1.2)	0.2(0.5)	0.6(1.8)	1.9(5.8)	1.1(2.5)	3.8(8.1)	0.4(0.9)	1.9(4.4)	0.8(1.9)	0.6(1.4)
SWCHN	0.2(0.5)	0.5(1.5)	1.0(2.9)	0.4(1.2)	0.1(0.1)	0.8(1.7)	4.7(9.2)	1.7(3.8)	0.1(0.2)	0.1(0.2)
CHN[a]	14.2(43)	12.9(37)	20.4(59.1)	9.3(28.9)	6.3(14.6)	5.5(11.9)	7.1(13.7)	8.2(18.3)	4.7(10.9)	3.4(7.1)
Korea	0.1(0.3)	0.1(0.1)	0.02(0.1)	0.03(0.1)	0.6(1.3)	0.0(0.0)	0.0(0.0)	0.1(0.1)	3.4(8.0)	0.7(1.5)
Japan	0.1(0.2)	0.04(0.1)	0.0(0.0)	0.0(0.0)	0.1(0.3)	0.0(0.0)	0.0(0.0)	0.0(0.0)	0.3(0.7)	2.7(5.7)
Ocean	5.8(17.4)	10.4(29.9)	2.6(7.6)	0.9(2.8)	3.4(7.8)	0.3(0.7)	1.7(3.3)	2.1(4.7)	8.2(19.1)	9.1(19.3)
Other	0.8(2.3)	2.6(7.5)	0.9(2.5)	1.3(4.1)	2.5(5.8)	4(8.7)	12(23.3)	5.4(12.0)	1.4(3.3)	1.8(3.9)
Total	33.2	34.9	34.5	32.2	43.2	46.4	51.7	44.5	43.2	47

[a] CHN denotes the whole of China, including ECHN, CCHN, NCHN, NECHN, NWCHN, and SWCHN.

winter monsoon, the O_3 outflow band shifted northwardly to 35°–45°N with a magnitude of 2×10^{-5} mol/(m^2 s), and ozone decreased by 5–10 ppbv south of 25°N. In summer, high surface ozone was constrained between 30° and 40°N in China, whereas ozone decreased to 10–30 ppbv in southern China, Korea, Japan, and the Pacific. This change was a combined result of intensive photochemical production and transport of clear maritime air masses by the summer monsoon, as reported by previous studies (Li et al., 2007; Nagashima et al., 2010; Itahashi et al., 2013). Note that because competition between Asian continental and maritime air masses in Japan was insufficiently represented in the model, ozone mixing ratios in Korea and Japan and the contributions of trans-boundary transport of Chinese emissions were overestimated, as has been found in several global models (Nagashima et al., 2010; Fiore et al., 2009). In fall, ozone showed a pattern similar to that in spring.

Tables 2–5 list the detailed source–receptor relationships of tagged regions in East Asia. Long-range contributions from outside East Asia (lateral and boundary conditions) to the Korean peninsula and Japan exhibited a winter-maximum and summer-minimum seasonal variation. In spring and winter, when surface ozone reached a maximum in the Korean peninsula and Japan, its contribution could be considered dominant (70%–80%). In summer, photochemical production became more important over East Asia. Local production contributed 8.6 ppbv (23.9%) in the Korean peninsula, which was 1.5 times the amount of trans-boundary transport from China. As for Japan, its self-contribution was 7.0 ppbv (24%) in summer, whereas trans-boundary transport from China was 1.6 ppbv. In China, the self-contribution in summer was 39.1%, which was three times than that in winter.

Ozone produced in the Pacific Ocean also contributed considerably to air pollution over the northwestern Pacific. This ozone, which was produced on the basis of precursors from China, the Korean peninsula, Japan, and Southeast Asia, showed a summer maximum and a winter minimum. In summer, ozone produced in the Pacific Ocean contributed 15.7, 14.7, and 2.7 ppbv respectively in the Korean peninsula, Japan, and China. In winter, this contribution was only 0.7–2.8 ppbv. This summer-maximum pattern was caused by the intensive solar heat flux and the strong southerly summer monsoon, which promoted northward transport of ozone precursors from Southeast Asia, China, the Korean peninsula, and Japan.

Fig. 8 shows the seasonal contributions of the targeted regions to various levels of surface daily ozone (0–100 ppbv, 2 ppbv per bin) in each grid cell within the Korean peninsula and in western and eastern Japan. Clearly, in spring and winter, long-range transport from outside East Asia dominated each ozone bin (0–100 ppbv). In summer, self-contributions in the Korean peninsula increased with ozone concentration, reaching 50%–60% at extra-high ozone concentrations (80 ppbv). This implied that controlling itself emissions would be an effective way to reduce summer ozone pollution episodes in the Korean peninsula. Unlike self-contributions, the contribution from the Pacific Ocean decreased with increasing ozone concentration in Korea. Peaks of trans-boundary transport from China appeared at 40–50 ppbv with a magnitude of 10%–15%.

In western and eastern Japan, as in Korea, long-range transport from outside East Asia contributed ~70% to each ozone bin in all seasons except summer. In summer, self-contributions at high ozone levels (60–100 ppbv) showed a slightly higher increase (30%–40%) than those at 0–40 ppbv (20%–30%). Transport of ozone produced in China was in the range of ~5%, which was less than in spring. This difference was caused by the East Asian monsoon climate. Although photochemical intensity increased in North China in summer, maritime air masses

Table 3
Surface ozone contributions (ppbv) and percentages (in brackets) from source regions to receptor regions over East Asia in summer 2010.

S/R	ECHN	SCHN	CCHN	NCHN	NECHN	NWCHN	SWCHN	CHN[a]	Korea	Japan
Boundary	3.4(9.2)	4.5(14.9)	3.8(8.7)	6(13.4)	8.3(24)	22.8(55.1)	21.6(47.2)	16.9(41)	4.6(12.7)	4.8(16.2)
ECHN	20.8(55.9)	1.0(3.2)	5.3(12.3)	5.4(12.1)	2.0(5.7)	0.7(1.6)	0.2(0.5)	2.8(6.9)	1.8(5.1)	0.5(1.6)
SCHN	2.0(5.3)	10.8(35.9)	4.2(9.7)	0.6(1.4)	0.2(0.5)	0.3(0.8)	1.0(2.2)	1.4(3.5)	0.3(0.8)	0.1(0.4)
CCHN	2.4(6.4)	1.5(5.1)	22.5(52.5)	7.3(16.3)	0.5(1.4)	1.3(3.2)	0.9(1.9)	2.7(6.6)	0.3(0.9)	0.1(0.3)
NCHN	0.4(1.1)	0.1(0.2)	0.7(1.7)	17.0(37.9)	1.2(3.5)	1.1(2.6)	0.1(0.1)	1.3(3.1)	0.6(1.6)	0.1(0.5)
NECHN	0.1(0.3)	0.02(0.1)	0.05(0.1)	0.3(0.7)	10.2(29.5)	0.3(0.8)	0.0(0.0)	1.0(2.3)	2.5(6.9)	0.6(2.2)
NWCHN	0.1(0.3)	0.03(0.1)	0.6(1.3)	2.6(5.7)	1.4(3.9)	8(19.4)	0.6(1.4)	3.8(9.2)	0.3(0.8)	0.1(0.4)
SWCHN	0.1(0.2)	0.3(1.0)	1.0(2.3)	0.7(1.5)	0.1(0.2)	2.1(5.0)	7.9(17.3)	3.0(7.4)	0.04(0.1)	0.02(0.1)
CHN[a]	25.8(69.5)	13.7(45.6)	34.3(79.9)	33.9(75.4)	15.5(44.8)	13.8(33.4)	10.7(23.4)	16.1(39.1)	5.8(16.1)	1.6(5.5)
Korea	0.2(0.5)	0.02(0.1)	0.1(0.1)	0.1(0.3)	1.2(3.6)	0.04(0.1)	0.0(0.0)	0.1(0.3)	8.6(23.9)	0.6(2.2)
Japan	0.2(0.4)	0.04(0.1)	0.1(0.2)	0.1(0.2)	0.2(0.7)	0.02(0.1)	0.0(0.0)	0.1(0.1)	0.7(1.9)	7.0(24.0)
Ocean	6.9(18.6)	7.7(25.4)	3.2(7.6)	3.7(8.3)	7.5(21.7)	0.9(2.3)	1.6(3.4)	2.7(6.7)	15.7(43.6)	14.7(50.2)
Other	0.7(1.8)	4.2(13.9)	1.5(3.5)	1.0(2.3)	1.8(5.3)	3.7(9.1)	11.9(26)	5.2(12.7)	0.6(1.8)	0.6(2.0)
Total	37.2	30.1	42.9	44.9	34.6	41.3	45.7	41.2	35.9	29.4

[a] CHN denotes the whole of China, including ECHN, CCHN, NCHN, NECHN, NWCHN, and SWCHN.

Table 4
Surface ozone contributions (ppbv) and percentages (in brackets) from source regions to receptor regions over East Asia in fall 2010.

S/R	ECHN	SCHN	CCHN	NCHN	NECHN	NWCHN	SWCHN	CHN[a]	Korea	Japan
Boundary	6.9(25.6)	5.8(17.2)	5.6(19.7)	11.4(48)	19.5(65.7)	27.1(73)	19.6(48.9)	19.8(56.1)	14.7(48.7)	18.7(55.8)
ECHN	13.4(50)	4.1(12)	4.2(14.9)	1.3(5.5)	0.7(2.2)	0.2(0.5)	0.4(1)	1.9(5.4)	1(3.3)	0.5(1.4)
SCHN	0.3(1.1)	11.7(34.7)	0.7(2.6)	0.1(0.3)	0(0)	0.1(0.2)	0.9(2.1)	1(2.8)	0(0.1)	0(0)
CCHN	0.9(3.5)	4.7(14)	14.5(51)	1.7(7.4)	0.2(0.5)	0.5(1.4)	1.5(3.8)	1.9(5.4)	0.2(0.7)	0.1(0.4)
NCHN	0.3(1.1)	0.1(0.4)	0.4(1.5)	5.5(23.3)	0.5(1.6)	0.3(0.9)	0.1(0.2)	0.5(1.3)	0.4(1.3)	0.2(0.6)
NECHN	0.2(0.7)	0(0.1)	0.1(0.2)	0.2(0.8)	4.3(14.3)	0.1(0.2)	0(0)	0.4(1.1)	1.7(5.6)	1.1(3.4)
NWCHN	0.3(1.1)	0.3(0.7)	0.8(3)	2(8.5)	0.9(3)	4.5(12.2)	0.5(1.2)	2.3(6.5)	0.5(1.7)	0.5(1.4)
SWCHN	0.1(0.3)	0.8(2.3)	0.6(2.1)	0.3(1.2)	0(0.1)	1(2.6)	6.5(16.1)	2.2(6.2)	0(0.2)	0(0.1)
CHN[a]	15.5(57.8)	21.7(64.2)	21.4(75.2)	11.1(47)	6.5(21.9)	6.7(18)	9.8(24.4)	10.1(28.7)	3.9(12.7)	2.4(7.3)
Korea	0.2(0.8)	0.1(0.2)	0(0.2)	0(0.1)	0.7(2.4)	0(0)	0(0)	0.1(0.2)	5.3(17.6)	0.8(2.4)
Japan	0.1(0.4)	0.1(0.2)	0(0.1)	0(0)	0(0.1)	0(0)	0(0)	0(0)	0.2(0.7)	3.9(11.8)
Ocean	3.8(14.1)	4.8(14.3)	1(3.5)	0.6(2.5)	1.8(5.9)	0.3(0.7)	1.1(2.8)	1.2(3.4)	5.4(17.9)	6.4(19.2)
Other	0.3(1.3)	1.3(3.9)	0.4(1.3)	0.6(2.4)	1.2(4)	3.1(8.2)	9.5(23.8)	4(11.4)	0.7(2.4)	1.2(3.5)
Total	26.7	33.8	28.5	23.6	29.7	37.1	40.1	35.2	30.2	33.5

[a] CHN denotes the whole of China, including ECHN, CCHN, NCHN, NECHN, NWCHN, and SWCHN.

with less O_3 from the Indian Ocean and the southern Pacific prevailed in the northwestern Pacific and Japan, blocking transport of high concentrations of ozone in China. Compared with studies by Nagashima et al. (2010) who estimated S–R relationships using a global model with a similar tracer-tagged module, the authors' estimated contribution from China to Japan was less in summer. Overestimation of transboundary transport by global models partly accounted for a general overestimation of ozone in Japan.

3.4. Regional transport of surface ozone within China

To control air pollution in China effectively, the State Council of China, the national-level policymaker has proposed a joint prevention and control strategy in which various cities must take control measures under unified planning and coordination to prevent regional transport of pollutants. This strategy required a good understanding of the S–R relationships of pollutants within China. In this section, the origins of O_3 in sub-regions within China are investigated.

In winter, as a result of the prevailing strong winter monsoon in East Asia (Fig. 7d), northern China (NCHN, NECHN, and NWCHN) was dominated by long-range transport from northern boundaries and no significant regional transport between sub-regions (Table 5). This long-range transport was weaker further south and decreased to 28.9% in SCHN (Table 5). In addition, regional transport between areas of southern China (SCHN, CCHN, and ECHN) played an important role. For example, although self-contributions were the major source of the ozone winter maximum in SCHN in all source regions for chemically produced ozone (27.6%), regional transport from CCHN and ECHN still reached 7.1% and 7.8%, accounting for almost half of these regions' self-contributions (Table 5). Ozone produced in the Pacific Ocean also made significant contributions (17.9%) to ozone in SCHN, which represented the chemical production of its precursors from northern China, Korea, and Japan through regional transport. In CCHN and ECHN, regional transport from other sub-regions reached 12.5 and 6.4% respectively.

In spring, with the weak winter monsoon and enhanced solar radiation, the relative contribution of chemical production in NCHN played a more important role than in winter, although long-range transport from outside East Asia (lateral and top conditions) was still dominant (64%). NCHN's self-contribution increased to 11.5% from 7.7% in winter (Table 2). Regional transport from other sub-regions in China contributed 17.4% of ozone, which was twice the percentage in winter (8.1%). Unlike NCHN, self-contributions and regional transport from other regions of China in both CCHN and ECHN showed similar fractions to those in winter (Tables 2 and 5). In CCHN, self-contributions and regional transport contributed respectively 36% and 23.1% of ozone in spring. In ECHN, their contributions were 33% and 10% respectively. However, with regard to the origins of different ozone levels, CCHN and ECHN showed a great difference (Fig. 9). In CCHN, self-contributions increased with total surface O_3, reaching 60% at greater than 70 ppbv ozone, which indicated that local emissions control could effectively reduce high-ozone episodes. In ECHN, the maximum self-contributions appeared at 60–70 ppbv and then decreased to 20%–30% for extra-high ozone concentrations (80–100 ppbv), at which long-range transport from lateral and top boundaries became the predominant origin. In SCHN, the contribution of chemical production in China decreased to 37% from 46.2% in winter. This was likely caused by the incursion of maritime air masses from the Indian Ocean in late spring (April–May).

In summer, photochemical production became the dominant origin in most regions of China. In ECHN, CCHN, and NCHN, ozone produced in

Table 5
Surface ozone contributions (ppbv) and percentages (in brackets) from source regions to receptor regions over East Asia in winter 2010.

S/R	ECHN	SCHN	CCHN	NCHN	NECHN	NWCHN	SWCHN	CHN[a]	Korea	Japan
Boundary	8.6(45.3)	8.3(30.7)	6.6(35.3)	15.4(80.3)	27.9(86.3)	28.9(80.9)	25.5(63.1)	23.3(70.2)	21.8(74.9)	29.6(79.6)
ECHN	6.6(34.7)	1.9(7.1)	1.4(7.5)	0.1(0.3)	0.1(0.3)	0(0)	0.1(0.2)	0.8(2.4)	0.6(1.9)	0.5(1.3)
SCHN	0.5(2.5)	7.5(27.6)	0.9(5)	0(0.1)	0(0)	0(0)	0.5(1.2)	0.6(1.9)	0(0.1)	0(0)
CCHN	0.7(3.9)	2.1(7.8)	7.1(38.1)	0.2(0.8)	0(0.1)	0.1(0.2)	0.6(1.5)	0.8(2.4)	0.1(0.4)	0.1(0.3)
NCHN	0.1(0.4)	0(0.2)	0.1(0.5)	1.5(7.7)	0(0.1)	0(0.1)	0(0)	0.1(0.3)	0.1(0.3)	0.1(0.2)
NECHN	0.1(0.3)	0(0.1)	0(0)	0(0.1)	1.5(4.8)	0(0.1)	0(0)	0.1(0.4)	1.4(5)	1(2.8)
NWCHN	0.2(1)	0.2(0.6)	0.4(2.3)	1.2(6.4)	0.8(2.4)	2.2(6.3)	0.2(0.4)	1.1(3.5)	0.5(1.7)	0.6(1.5)
SWCHN	0.1(0.7)	0.8(2.9)	1(5.5)	0.1(0.4)	0(0.1)	0.3(0.8)	3.4(8.5)	1.1(3.4)	0(0.1)	0.1(0.1)
CHN[a]	8.2(43.4)	12.5(46.2)	11(58.9)	3(15.8)	2.5(7.8)	2.7(7.5)	4.8(11.9)	4.8(14.3)	2.8(9.5)	2.3(6.3)
Korea	0(0.1)	0(0.1)	0(0)	0(0)	0.2(0.7)	0(0)	0(0)	0(0.1)	1.7(5.9)	0.5(1.3)
Japan	0(0)	0(0)	0(0)	0(0)	0(0)	0(0)	0(0)	0(0)	0(0.1)	0.8(2.1)
Ocean	1.8(9.5)	4.9(17.9)	0.6(3.4)	0(0.2)	0.4(1.1)	0(0.1)	0.6(1.5)	0.7(2)	2.1(7.3)	2.8(7.7)
Other	0.3(1.7)	1.4(5.1)	0.4(2.3)	0.7(3.7)	1.3(4.1)	4.1(11.4)	9.5(23.6)	4.5(13.5)	0.7(2.3)	1.1(3)
Total	19	27.1	18.7	19.1	32.2	35.8	40.4	33.2	29.2	37.1

[a] CHN denotes the whole of China, including ECHN, CCHN, NCHN, NECHN, NWCHN, and SWCHN.

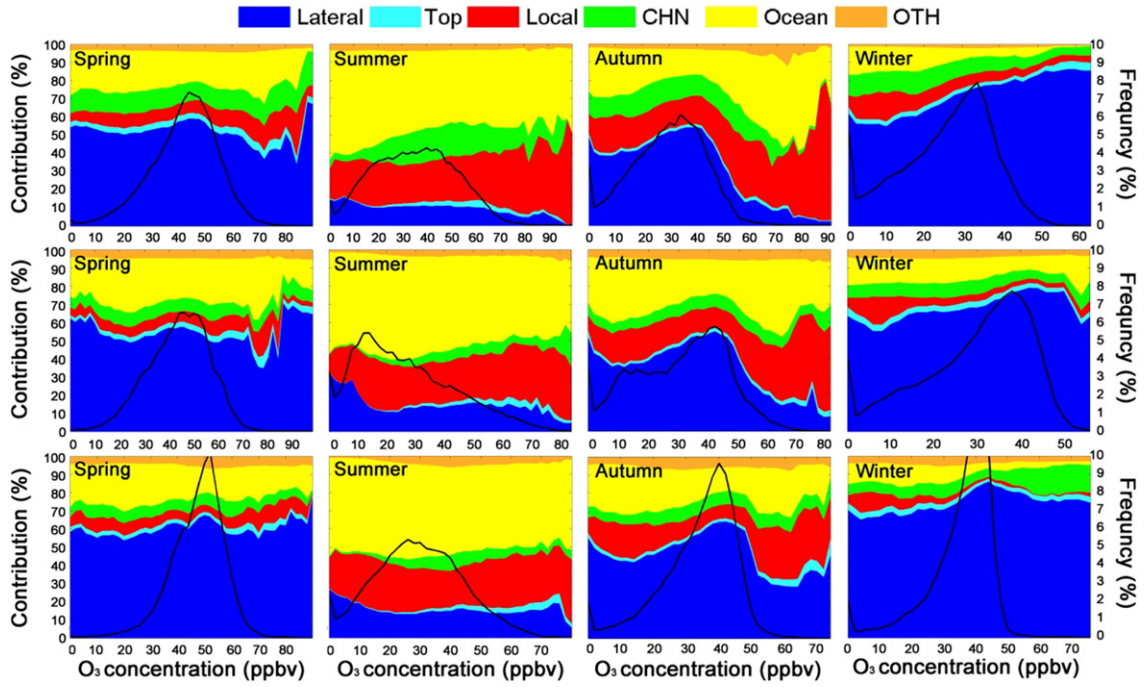

Fig. 8. Seasonal relative contributions of targeted regions to different levels of surface daily ozone (0–100 ppbv, 2 ppbv per bin) in each grid cell within the Korean peninsula (top), western Japan (middle) and eastern Japan (bottom). Local and CHN represent self-contributions and trans-boundary transport of O_3 produced in China. Top and Lateral represent contributions from the top and lateral boundaries of the simulation respectively. OTH represents the contribution of the remaining sources.

China reached 69.5%, 79.9%, and 75.4% of total ozone respectively. NCHN was the major receptor of regional transport within China, receiving 37.5% of its ozone from regional transport, including 16.3% and 12.1% from CCHN and ECHN respectively. The received ozone was even comparable with its self-contributions (37.9%). With the combined effects of local photochemistry and regional transport, ozone in NCHN became the highest in the whole of East Asia in summer. In CCHN, self-contributions and regional transport contributed 52.5% and 27.4% respectively. ECHN and SCHN were the two largest source regions under the influence of the southerly summer monsoon. Fig. 9 shows self-contributions and regional transport within China for different levels of surface daily ozone in ECHN, CCHN, and NCHN. It was found that self-contributions played a dominant role on high-ozone days (60–100 ppbv), whereas the influence of regional transport was constrained when ozone levels were below 60 ppbv.

In fall, ozone was transported southward into SCHN with the prevailing weak northerly winds. As shown in Table 4, CCHN and ECHN contributed 14% and 12% respectively of SCHN ozone, which was comparable with its self-contributions (34%). CCHN was another receptor of regional transport, receiving 14.9% of its ozone from ECHN.

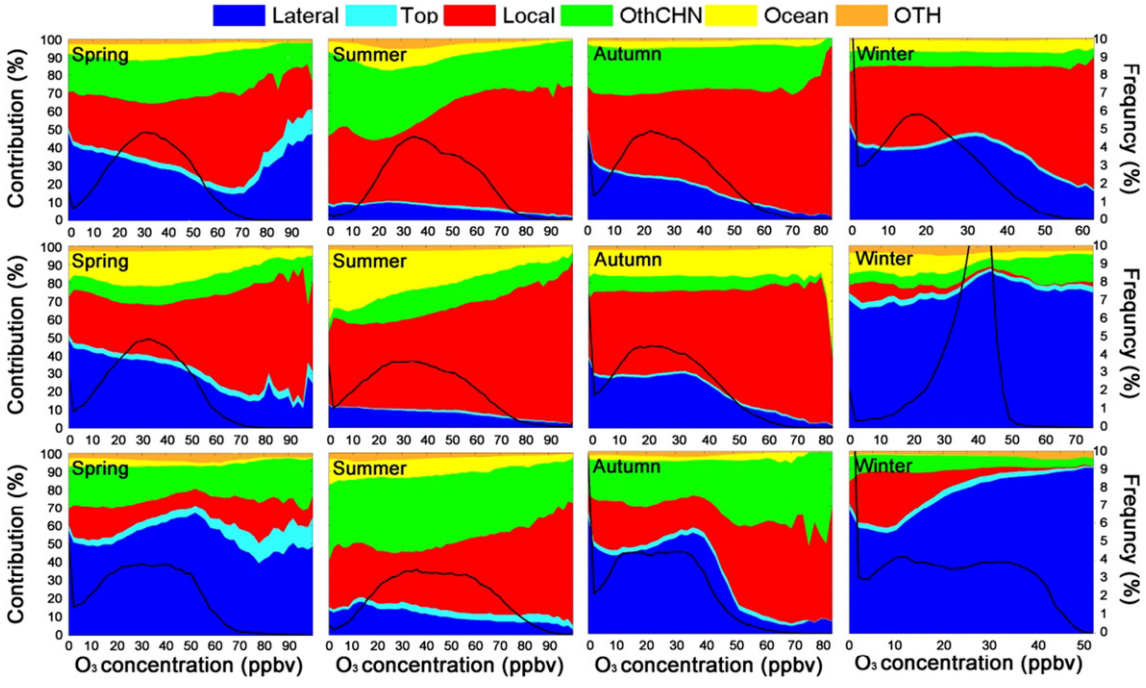

Fig. 9. The same as Fig. 8, but the receptor regions are CCHN (top), ECHN (middle), and NCHN (bottom). OthCHN represents the remaining parts of China excluding itself.

Unlike NCHN, ECHN, CCHN, and SCHN, ozone produced in NECHN, NWCHN, and SWCHN was rarely transported into other sub-regions in China, and these regions received few contributions from other regions in China. Note that SWCHN received ~20% of its ozone from India and Southeast Asia.

4. Conclusions

This study used a regional chemical transport model (NAQPMS) coupled with an on-line tracer-tagged procedure to simulate a full year of surface O_3 concentrations over East Asia. The aim of this research was to investigate quantitatively the long-term ozone S–R relationships over East Asia, with a special focus on ozone source regions at different levels of daily ozone mixing ratios. This effort should promote an understanding of the causes of long-term ozone trends in East Asia and an assessment of the effectiveness of the unprecedented "Atmospheric Pollution Prevention Action Plan". Comparison with ground and satellite data for ozone and its precursors has shown that the model reproduced seasonal variations in surface ozone and tropospheric NO_2 mean concentrations in East Asia reasonably well.

The results showed that self-contributions were strongly responsible for extra-high ozone levels (exceeding 80 ppbv) over Korean peninsula instead of long-range transport of outside East Asia, although the latter contributed the greatest fraction to annual surface ozone over most regions in East Asia (50–80%). The major cause was that long-range transport of outside East Asia was mainly limited to ozone concentrations below 60 ppbv. This indicated that controlling local emissions would be more effective in reducing summer ozone pollution episodes in the Korean peninsula. Different from Korea, self-contributions and photochemical production of precursors emitted by China, Korea, Japan, and Southeast Asia over the Pacific Ocean contributed the most to high ozone (60–85 ppbv) over western Japan, which indicated international joint-controls are needed.

Ozone source–receptor relationships showed high seasonal variability over East Asia. Long-range transport from outside East Asia to the Korean peninsula and Japan exhibited a winter-maximum and summer-minimum seasonal variation due to the Asian monsoon, whereas the relative contribution of photochemical production exhibited the reverse pattern. The seasonal pattern of long-range transport from outside East Asia resulted in the widespread spring-maximum in the Korean peninsula and Japan. In summer, self-contributions contributed 8.6 ppbv (23.9%) in the Korean peninsula, which was 1.5 times the trans-boundary transport from China. In Japan, self-contributions and trans-boundary transport from China accounted for 7.0 ppbv (24%) and 1.6 ppbv (5.5%) respectively. Ozone produced in the Pacific Ocean also contributed considerably to air pollution over the northwestern Pacific in summer. In China, self-contributions in summer accounted for 39.1%, or three times the percentage in winter.

Significant regional transport of surface ozone between sub-regions within China was observed in this simulation. In general, regional transport showed a north-to-south in winter and south-to-north in summer pattern under the East Asian monsoon climate. In winter, 18.6% ozone in SCHN came from the regional transport from ECHN and CCHN, which accounted for the distinctive wintertime-maximum pattern in SCHN. In summer, intensive regional transport blew ozone in ECHN and SCHN into NCHN (37.5% of ozone concentration) and partly resulted in that NCHN became the highest in the whole of East Asia in summer. These regional transports present a major challenge to policy-makers because most control measures to date have been restricted to particular regions.

Acknowledgments

This work is funded by the Chinese Academy of Sciences (CAS) Strategic Priority Research Program (Grant Nos. XDB05030100 and XDA05100501), Key Projects in the National Science & Technology Pillar Program (2014BAC06B03), Natural Science Foundation of China (NSFC) (41275138), National Key Project of Basic Research (2014CB447900), and China Ministry of Environmental Protection's Special Funds for Scientific Research on Public Welfare (201009002).

References

Ahamad, F., et al., 2014. Variation of surface ozone exceedance around Klang Valley, Malaysia. Atmos. Res. 139, 116–127.
Boersma, K.F., et al., 2011. An improved tropospheric NO_2 column retrieval algorithm for the Ozone Monitoring Instrument. Atmos. Meas. Tech. 4, 1905–1928.
Cao, G., Zhang, X., Wang, D., & Zheng, F., 2005. Inventory of atmospheric pollutants discharged from biomass burning in China continent. China Environ. Sci. 25 (4), 389–393 (in Chinese).
Fiore, A.M., et al., 2009. Multi-model estimates of intercontinental source–receptor relationships for ozone pollution. J. Geophys. Res. 114, D04301. http://dx.doi.org/10.1029/2008JD010816.
Ge, B., et al., 2014. Wet deposition of acidifying substances in different regions of China and the rest of East Asia: modeling with updated NAQPMS. Environ. Pollut. 187, 10–21.
Grewe, V., 2004. Technical note: a diagnostic for ozone contributions of various NOx emissions in multi-decadal chemistry-climate model simulations. Atmos. Chem. Phys. 4, 729–736.
Guenther, A., et al., 1995. A global model of natural volatile organic compound emissions. J. Geophys. Res. 100 (D5), 8873–8892.
Horowitz, L.W., et al., 2003. A global simulation of tropospheric ozone and related tracers: description and evaluation of MOZART, version 2. J. Geophys. Res. 108 (D24), 4784. http://dx.doi.org/10.1029/2002JD002853.
Itahashi, S., Uno, I., & Kim, S., 2013. Seasonal source contributions of tropospheric ozone over East Asia based on CMAQ–HDDM. Atmos. Environ. 70, 204–217. http://dx.doi.org/10.1016/j.atmosenv.2013.01.026.
James, F.S., & Malm, W.C., 2000. Spatial Distributions of Reconstructed Light Extinction and Light-Extinction Budgets. In: Malm, C.W. (Ed.), Spatial and Seasonal Patterns and Temporal Variability of Haze and its Constituents in the United States: Report III. USEPA, pp. 1–38.
Kurokawa, J., et al., 2013. Emissions of air pollutants and greenhouse gases over Asian regions during 2000–2008: Regional Emission inventory in Asia (REAS) version 2. Atmos. Chem. Phys. 13, 11019–11058. http://dx.doi.org/10.5194/acp-13-11019-2013.
Lee, S., Akimoto, H., Nakane, H., Kurnosenko, S., & Kinjo, Y., 1998. Lower tropospheric ozone trend observed in 1989–1997 at Okinawa, Japan. Geophys. Res. Lett. 25, 1637–1640.
Li, J., Wang, Z.F., Akimoto, H., Gao, C., Pochanart, P., & Wang, X.Q., 2007. Modeling study of ozone seasonal cycle in lower troposphere over east Asia. J Geophys Res-Atmos 112, D22S25. http://dx.doi.org/10.1029/2006JD008209.
Li, J., et al., 2008. Near-ground ozone source attributions and outflow in central eastern China during MTX2006. Atmos. Chem. Phys. 8, 7335–7351.
Li, J., Wang, Z., Akimoto, H., Tang, J., & Uno, I., 2009. Modeling of the impacts of China's anthropogenic pollutants on the surface ozone summer maximum on the northern Tibetan Plateau. Geophys. Res. Lett. 36, L24802. http://dx.doi.org/10.1029/2009GL041123.
Li, J., et al., 2011. Impacts of aerosols on summertime tropospheric photolysis frequencies and photochemistry over Central Eastern China. Atmos. Environ. 45, 1817–1829.
Li, J., et al., 2012. Mixing of Asian mineral dust with anthropogenic pollutants over East Asia: a model case study of a super-duststorm in March 2010. Atmos. Chem. Phys. 12, 7591–7607.
Li, J., et al., 2013. Assessing the effects of trans-boundary aerosol transport between various city clusters on regional haze episodes in spring over East China. Tellus B. 65, 20052. http://dx.doi.org/10.3402/tellusb.v65i0.2005.
Madronich, S., 1989. Photodissociation in the atmosphere 1. Actinic flux and the effect of ground reflections and clouds. J. Geophys. Res. 92, 9740–9752.
Nagashima, T., Ohara, T., Sudo, K., & Akimoto, H., 2010. The relative importance of various source regions on East Asian surface ozone. Atmos. Chem. Phys. 10, 11305–11322.
Naja, M., & Akimoto, H., 2004. Contribution of regional pollution and long-range transport to the Asia-Pacific region: analysis of long-term ozonesonde data over Japan. 109 p. D21306. http://dx.doi.org/10.1029/2004JD004687.
Nenes, A., Pandis, S.N., & Pilinis, C., 1998. ISORROPIA: a new thermodynamic equilibrium model for multiphase multicomponent inorganic aerosols. Aquat. Geochem. 4, 123–152.
Odum, J.R., Jungkamp, T., Griffin, R.J., Flagan, R.C., & Seinfeld, J.H., 1997. The atmospheric aerosol-forming potential of whole gasoline vapor. Science 276, 96–99.
Skamarock, W.C., & Klemp, J.B., 2008. A time-split nonhydrostatic model for weather research and forcasting applications. J. Comput. Phys. 22 (7), 3465–3485.
Stammes, P., 2001. Spectral Radiance Modeling in the UV-Visible Range, IRS2000. In: Smith, W.L., Timofeyev, Y.M. (Eds.), Current Problems in Atmospheric Radiation. A. Deepak Publ, Hampton (VA), pp. 385–388.
Tang, Y., et al., 2003. Influences of biomass burning during the Transport and Chemical Evolution Over the Pacific (TRACE-P) experiment identified by the regional chemical transport model. J. Geophys. Res. 108 (D21), 8824. http://dx.doi.org/10.1029/2002JD003110.

Waleck, C.J., & Aleksic, N.M., 1998. A simple but accurate mass conservative peak-preserving, mixing ratio bounded advection algorithm with Fortran code. Atmos. Environ. 32, 3863–3880.
Wang, Z., Maeda, T., Hayashi, M., Hsiao, L.F., & Liu, K.Y., 2001. A nested air quality prediction modeling system for urban and regional scales, application for high-ozone episode in Taiwan. Water Air Soil Pollut. 130, 391–396.
Wesely, M.L., 1989. Parameterization of surface resistances to gaseous dry deposition in regional-scale numerical models. Atmos. Environ. 23, 1293–1304.
Wild, O., & Akimoto, H., 2001. Intercontinental transport of ozone and its precursors in a three-dimensional global CTM. J. Geophys. Res. 106 (D21), 27,729–27,744.
Wild, O., & Prather, M.J., 2006. Global tropospheric ozone modeling: quantifying errors due to grid resolution. J. Geophys. Res. 111, D11305. http://dx.doi.org/10.1029/2005JD006605.
Wu, R.G., 2002. A mid-latitude Asian circulation anomaly pattern in boreal summer and its connection with the Indian and East Asian summer monsoons. Int. J. Climatol. 22, 1879–1895.
Xin, J.Y., et al., 2010. Variability and reduction of atmospheric pollutants in Beijing and its surrounding area during the Beijing 2008 Olympic Games. Chin. Sci. Bull. 55, 1937–1944.
Xu, X., et al., 2008. Long-term trend of surface ozone at regional background station in eastern China 1991–2006: enhanced variability. Atmos. Chem. Phys. 8, 2595–2607.
Yamaji, K., et al., 2006. Analysis of the seasonal variation of ozone in the boundary layer in East Asia using the community multi-scale air quality model: what controls surface ozone levels over Japan? Atmos. Environ. 40, 1856–1868.
Zaveri, R.A., & Peters, L.K., 1999. A new lumped structure photochemical mechanism for large-scale applications. J. Geophys. Res. 104, 30,387–30,415.
Zhang, R., Sarwar, G., Fung, J., & Lau, A., 2013. Role of photoexcited nitrogen dioxide chemistry on ozone formation and emission control strategy over the Pearl River Delta, China. Atmos. Res. 132–133, 332–344.
Zhao, B., et al., 2013. Environmental effects of the recent emission changes in China: implications for particulate matter pollution and soil acidification. Environ. Res. Lett. 8, 24–31.